Accuracy of Non-invasive Frequency Estimation during Atrial Fibrillation

Jorge Pedrón-Torrecilla[1], Alejandro Liberos[1], José Millet[1], Andreu M Climent[2], María S Guillem[1]

[1]Bio-ITACA, Universitat Politècnica de València, Valencia, Spain
[2]Hospital General Universitario Gregorio Marañón, Madrid, Spain

Abstract

Ablation procedures have become one of the most efficient treatments for termination of atrial fibrillation (AF). The aim of this study is to evaluate the accuracy of dominant frequency (DF) maps on the epicardium computed from non-invasive recordings as a clinical tool for the identification of AF sources.

Spherical and realistic atrial models were used. Four fibrillation patterns with varying dominant frequency distributions were obtained. Surface potentials were computed by solving the forward problem and adding noise at signal-to-noise ratios (SNR) from 10 to 20 dB.

For the spherical model, with 80% of the surface with a DF of 14 Hz and 20% with a DF of 21.5 Hz, RDM between generated and inverse computed potentials was 0.56 without added noise and 1.05 with SNR=10 dB. However, for the same conditions, the RDM* of DF maps were 0.02 and 0.09, with DF errors of 0.01±0.31 Hz and 0.26±1.39 Hz, respectively. For the realistic model, frequency reconstruction was consistent with generated electrograms, allowing an accurate estimation of the DF distribution with a maximum RDM* of 0.19 (SNR=10dB).*

Inverse computed DF maps reconstructed during in-silico AF were more accurate than voltage maps. Non-invasive estimation of DF maps during AF is feasible and may help in procedure planning.

1. Introduction

Atrial fibrillation (AF) has a great clinical impact in morbidity and mortality in developed countries [1]. Treatment with antiarrhythmic drugs is not always effective and has many secondary effects. These limitations have led to the development of new therapeutic strategies, such as radiofrequency ablation with current success rates in arrhythmia control of 50 to 80 % [1]. Therefore, radiofrequency ablation is currently one of the most widely used in clinical practice and has shown to be especially effective in patients with an activation frequency gradient when targeting high frequency sites [2,3].

Although electroanatomical cardiac mapping can be used to detect stable foci in the atria or to characterize a re-entrant pattern during atrial flutter, location of atrial sources during AF is more complicated since contact mapping is performed sequentially. A non-invasive reconstruction of the atrial activation sequence based on the recording of multiple simultaneous ECGs may overcome this limitation.

Patterns of activation during atrial arrhythmias computed by non-invasive imaging have already been reported [4,5]. However, solution of the inverse problem could not be validated with epicardial signals.

Our hypothesis is that non-invasive identification of the regions initiating and maintaining AF and, therefore, the ablation process targets, is possible by solving the inverse problem of the electrocardiography.

In this article, we aim to validate DF maps computed by solving the inverse problem of the electrocardiography with epicardial dominant frequency maps generated with mathematical AF models at which frequencies in the entire atria are known. We will also determine the sensitivity to noise of the inverse problem solution in terms of their voltage distributions and their DF maps.

2. Methods

2.1. Inverse problem resolution

In order to obtain the potentials on the heart surface from the potentials recorded non-invasively from the torso surface of the patient, we solved the inverse problem of the electrocardiography by using the Boundary Element Method (BEM).

According to the BEM formulation [6-9], potentials on the surface of the torso can be computed from potentials on the heart surface by using (1)-(3):

$$A_1 x = b \tag{1}$$

$$A_1 = \begin{pmatrix} D_{HH(nxn)} & G_{HH(nxn)} \\ D_{TH(mxn)} & G_{TH(mxn)} \end{pmatrix}, \quad x = \begin{pmatrix} \Phi_H \\ \Gamma_H \end{pmatrix},$$

$$b = \begin{pmatrix} -D_{HT(nxm)}\Phi_T \\ -D_{TT(mxm)}\Phi_T \end{pmatrix} \tag{2}$$

$$\Phi_T = A\Phi_H = \left(D_{TT} - G_{TH}G_{HH}^{-1}D_{HT}\right)^{-1} \cdot \left(G_{TH}G_{HH}^{-1}D_{HH} - D_{TH}\right)\Phi_H \quad (3)$$

where Φ_H is the potential on the surface of the heart, Φ_T is the potential on the surface of the torso, Γ_H is the potential gradient of the heart, D_{XY} is the potential transfer matrix from point Y to point X, and G_{XY} is the potential gradient transfer matrix from point Y to point X.

The inverse problem can be solved by computing the inverse of matrix A (A^{-1}). However, A^{-1} is ill-conditioned and, in order to overcome the ill-conditioned nature of A^{-1}, the system needs to be regularized. This regularization can be accomplished by using Tikhonov's method, which consists of a minimization problem (4):

$$\min_{x \in E^n} \left\{ \left\| A\Phi_H - \Phi_T \right\|^2 + t \left\| B\Phi_H \right\|^2 \right\} \quad (4)$$

where t is a regularization parameter that can be obtained with the L-curve method and B is the spatial regularization matrix which is the identity matrix (zero-order). Therefore, the inverse problem can be solved by using the expression (5):

$$\Phi_H(t) = \left(A'A + tB'B\right)^{-1} A'\Phi_B \quad (5)$$

2.2. Inverse problem validation

Several surface potential distributions were calculated by solving the forward problem of the electrocardiography, using a spherical model for the atria and the torso and a realistic model. Spherical atrial model was constituted by 163842 nodes and a radius of 5 cm. Realistic atria consisted of 577264 nodes and its size was 12.5x9 cm [10]. The action potential of each node was simulated by using a mathematical model which includes ionic currents, pumps and exchangers, and processes regulating intracellular concentration changes of Na^+, K^+ and Ca^{2+} [11]. The whole tissue is described as a monodomain model. After discretization of the spatial derivatives for an isotropic medium, the evolution of the transmembrane voltage of each cell (i.e. V_i for the i-th cell) V_i, was controlled by the following first-order, time-dependent ordinary differential equation:

$$\frac{dV_i}{dt} = \frac{I_{total,i}}{C_m} - D\sum_j \frac{V_i - V_j}{d_{i,j}} \quad (6)$$

where D describes the diffusion of voltage through the medium, $I_{total,i}$ summarizes the contribution of all transmembrane currents [11], C_m is the transmembrane capacitance, and $d_{i,j}$ is the distance between neighbor cells i and j.

Atrial fibrillation in the realistic model was induced in-silico by a S1-S2 stimulation protocol. Two S1 stimulations with a period of 100 ms and a pulse duration of 5 ms were applied at either the left superior pulmonary veins or the sinus node, depending on the desired pattern. A rectangular shape stimulus S2 was applied 70 ms after the last S1 stimulus with a duration of 2 ms in the same S1 pacing site, inducing the AF. The model incorporated an extra potassium current, the acetylcholine (ACh) potassium current (IKacg). This current produces a shortening in the action potential which favors the occurrence of arrhythmic behavior and the presence of different activation frequencies [12].

Mathematical computations were performed by using an adaptive time-step solver on a Graphical Processing Unit [13]. Transmembrane potentials were computed for a simulation time of 5 seconds after stabilization of the model and were resampled to 1 kHz.

Simulated electrograms (EGMs) (i.e. 2562 signals for the spherical model and 5988 signals for the realistic atria) were calculated by using transmembrane potentials generated by the cellular mathematical model [10]:

$$EGM = \sum_{\vec{r}} \left(\frac{\vec{r}}{r^3} \right) \cdot \vec{\nabla} V_m \quad (7)$$

where $\vec{r}$ is the distance vector between the measuring point and a point in the tissue domain (r is the euclidean distance -1 mm-), $\vec{\nabla}$ denotes the gradient operator, and V_m is the transmembrane potential.

Body surface potential signals were computed on the outer surface from EGMs by solving the forward problem [6-9]. Specifically, ECGs on a spherical torso model with radius 15 cm with 642 nodes and 1280 faces, and on a realistic torso model with 771 nodes and 1538 faces were estimated [14,15].

Simulated ECGs with and without added white noise at different signal-to-noise ratios (SNR 20 dB, 10 dB) were used to reconstruct epicardial EGMs by solving the inverse problem as described in section 2.1.

Frequency analysis was performed by computing the power spectral density of all signals by using Welch's periodogram with a Hamming window of 2 seconds and 50 % overlap, with 4096 FFT points per window.

Accuracy of reconstructed electrograms was quantified by measuring the RDM* and the DF error (mean ± standard deviation) both on the reconstructed potential maps and on DF maps:

$$RDM^* = \sqrt{\sum_n \left(\frac{\phi_H}{\sqrt{\sum_n \phi_H^{\,2}}} - \frac{\phi_{H-PI}}{\sqrt{\sum_n \phi_{H-PI}^{\,2}}} \right)^2} \quad (8)$$

where ϕ_H and $\phi_{H\text{-}PI}$ are the values of the potentials or dominant frequencies for the original electrograms and for the computed electrograms by solving the inverse problem of the electrocardiography; n is the number of nodes of the atria model.

3. Results

3.1. Sphere model

In Fig.1, the voltage and frequency reconstructions with the spherical model at varying SNRs are depicted. With no added noise, inverse computed EGMs allow an accurate estimation of propagation dynamics which is reflected in a low RDM* value 0.56. However, the accuracy of the solution decreases progressively with increasing noise levels (RDM* values of 0.99 and 1.05 for SNRs of 20 and 10 dB respectively).

DF frequency maps show that 20 % of the sphere (which harbors a dominant rotor) is activated at a frequency of 21.5 Hz whereas the remaining 80 % of the sphere was activated at a frequency of 14 Hz. With no added noise DF map can be estimated with almost no error (RDM* equal to 0.02 and 0.01 Hz mean DF error). Accuracy decreased slightly with increasing added noise levels, but in this case the accuracy is higher and less sensitive to noise than in the voltage domain (RDM* equal to 0.06 and 0.09 for SNRs of 20 and 10 dB respectively and DF errors of 0.14 and 0.26 Hz).

3.2. Realistic model

DF maps computed for the realistic atrial and torso models are depicted in Fig.2. Resulting AF patterns were: (1) AF generated by a rotor located in the left atrium (LA), with a DF of 12.25 Hz in the LA and 8 Hz in the RA, (2) AF generated by a rotor located in the RA, with a DF of 12.25 Hz in the RA and 8 Hz in the LA and (3) AF generated by a rotor located in the LA with no DF gradient (12.25 Hz both in the RA and LA). Errors in estimation of the DF map with added noise at a SNR of 10 dB was 1.00±1.71 Hz, 0.79±1.62 Hz and 0.10±0.12 Hz for models 1, 2 and 3 respectively. Measured RDM* values of the frequency maps in the realistic model were 0.19, 0.17 and 0.01, however, RDM* values of the potential distribution were 1.40, 1.43 and 1.43, respectively. Dominant frequency maps were accurately reconstructed and the case with no frequency gradient was correctly identified.

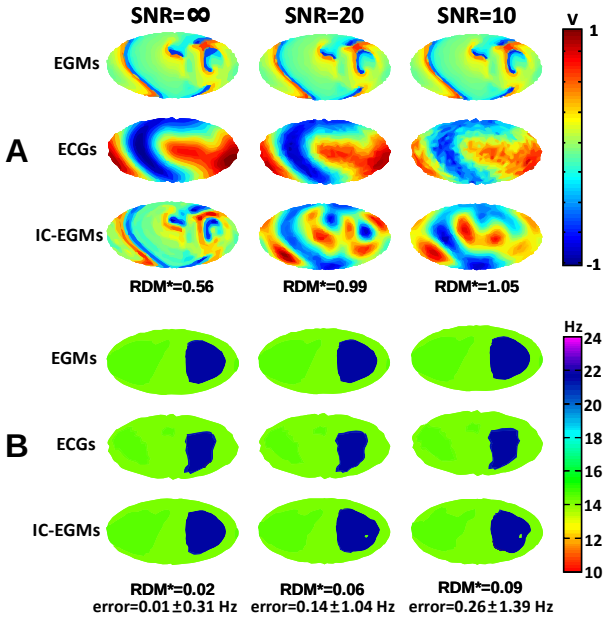

Figure 1: Inverse problem resolution for the model of concentric spheres at different SNRs (Aitoff cartographic representation). Panel A, examples of voltage maps for the EGMs computed from the transmembrane potentials, surface potentials (ECGs) and inverse computed EGMs (IC-EGMs). Panel B, DF maps.

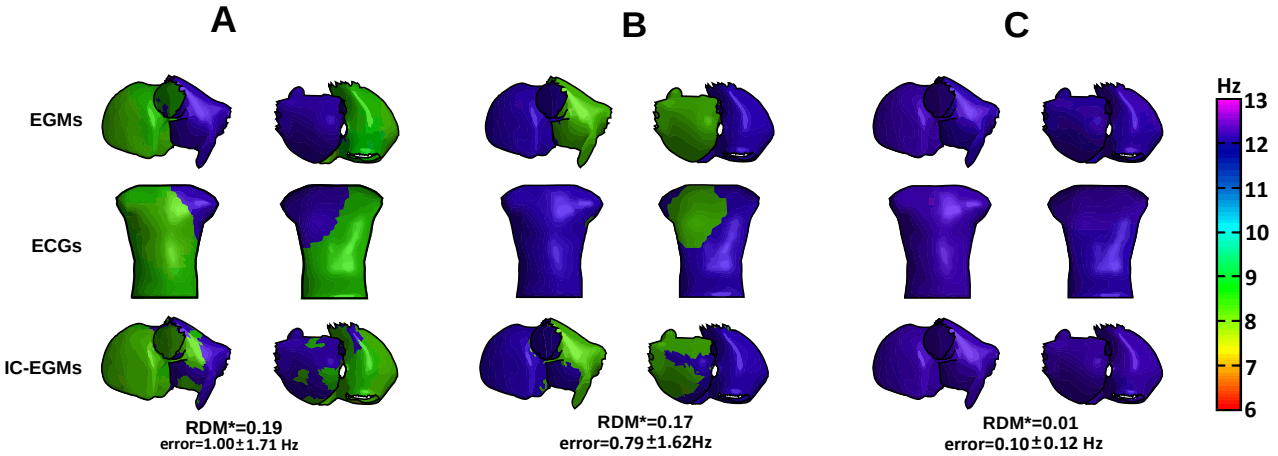

Figure 2: DF maps reconstructed by the inverse problem resolution for 10 dBs signal-to-noise ratios in a realistic torso model. Panel A, AF generated by a rotor located in the LA, with a frequency of 12.25 Hz in the LA and 8 Hz in the RA; Panel B, AF generated by a rotor located in the RA, with a frequency of 12.25 Hz in the RA and 8 Hz in the LA; Panel C, AF generated by a rotor located in the LA, without a frequency gradient with 12.25 Hz in the RA and in the LA.

4. Discussion and conclusion

In the present study, noninvasive reconstruction of the frequency map in the atria was validated by using mathematical models and the inverse problem of the electrocardiography.

Mathematical simulations were used to quantify the accuracy of reconstructed activation sequences. By using this detailed ionic model of the atria, different clinical scenarios could be simulated (i.e. AF maintained by functional rotors at different locations and with different DF patterns) and could be used to evaluate the accuracy of the inverse problem resolution, to estimate propagation patterns and frequency maps, and to clarify the relation between epicardial propagation patterns and its representation on the torso [3].

This work validated the non-invasive location of the dominant frequency maps which may be useful for planning an ablation procedure in atrial fibrillation patients. During the last years, different groups have developed and tested the methodology to noninvasively reconstruct the epicardial activation sequence during atrial fibrillation in the time domain [5], however, a non-invasive frequency map during AF is a new technique which needed to be validated. This study showed how frequency maps were accurately reconstructed for different AF patterns, locating the dominant frequency regions and detecting when there is no frequency gradient. Estimation of DF maps has also shown to be less sensitive to noise than estimation of propagation patterns based on measured voltages and thus more robust for detecting electrical sources during AF.

This method demonstrated to be a promising tool for the non-invasive mapping of the frequency maps during atrial fibrillation and may help in planning ablation procedures.

Acknowledgements

This work was partially supported by Spanish Ministry of Education (FPU-2012), "Universitat Politècnica de València" (PAID-2009-2012 and PAID-05-12) and the "Generalitat Valenciana" (GV/2012/039).

References

[1] Calkins H, Brugada J, Packer DL, et al. HRS/EHRA/ECAS Expert consensus statement on catheter and surgical ablation of atrial fibrillation: Recommendations for personnel, policy, procedures and follow-up. Heart Rhythm 2007;4:816-61.

[2] Atienza F, Almendral J, Jalife J, Zlochiver S, Ploutz-Snyder R, Torrecilla E, Arenal A, Kalifa J, Fernandez Aviles F, Berenfeld O. Real-time dominant frequency mapping and ablation of dominant frequency sites in atrial fibrillation with left-to-right frequency gradients predicts long-term maintenance of sinus rhythm. Heart Rhythm 2009;6:33-40.

[3] Guillem MS, Climent MC, Millet J, Arenal A, Fernandez-Aviles F, Jalife J, Atienza F, Berenfeld O. Noninvasive localization of maximal frequency sites of atrial fibrillation by body surface potential mapping. Circ Arrhythm Electrophysiol 2013;6:00-00.

[4] Roten L, Pedersen M, Pasacale P, Shah A, Eliautou S, Scherr D, Sacher F, Haïssaguerre M. Noninvasive electrocardiographic mapping for prediction of tachycardia mechanism and origin of atrial tachycardia following bilateral pulmonary transplantation. J Cardiovasc Electrophysiol 2012;23(5):553-5.

[5] Cuculich PS, Wang Y, Lindsay BD, Faddis MN, Schuessler RB, Damiano Jr RJ, Li L, Rudy Y. Noninvasive characterization of epicardial activations in humans with diverse atrial fibrillation patterns. Circulation 2010;122:1364-72.

[6] Stenroos M. The transfer matrix for epicardial potential in a piece-wise homogeneous thorax model: boundary element formulation. Phys Med Biol 2009;54:5443-55.

[7] Horácek BM, Clements JC. The inverse problem of electrocardiography: a solution in terms of single- and double-layer sources on the epicardial surface. Math Bios 1997;144:119-54.

[8] De Munck J.C. A linear Discretization of the Volume Conductor Boundary Integral Equation Using Analytically Integral Elements. IEEE Trans on Biomed Eng 1992;39(9):986-90.

[9] Cowper GR. Gaussian quadrature formulas for triangles. Int J Num Meth Eng 1972;7(3):405-8.

[10] Harrild DM, Henriquez CS. A computer model of normal conduction in the human atria. Circ Res 2000;87:E25-E36.

[11] Courtemanche M, Ramirez R.J, Nattel S. Ionic mechanisms underlying human atrial action potential properties: Insights from a mathematical model. Am J Physiol -Heart Circul Physiol 1998;275:H301-H321.

[12] Atienza F, Almendral J, Moreno J, Vaidyanathan R, Talkachou A, Kalifa J, Arenal A, Villacastin JP, Torrecilla EG, Sanchez A, Ploutz-Synder R, Jalife J, Berenfeld O. Activation of inward rectifier potassium channels accelerates atrial fibrillation in humans - evidence for a reentrant mechanism. Circulation 2006; 114:2434-42.

[13] Garcia VM, Liberos A, Climent AM, Vidal A, Millet J, González A. An adaptive step size GPU ODE solver for simulating the electric cardiac activity. Computing in Cardiology 2011;38:233-6.

[14] MacLeod RS, Johnson CR, Ershler PR. Construction of an inhomogeneous model of the human torso for use in computational electrocardiography. 13th Ann Int Conf, IEEE Eng Med and Biol Soc 1991;1991:688-9.

[15] Pedrón-Torrecilla J, Climent A, Liberos A, Pérez-David E, Millet J, Atienza F, Guillem MS. Non-invasive estimation of the activation sequence in the atria during sinus rhythm and atrial tachyarrhythmia. Computing in Cardiology 2012; 39:901-4.

Address for correspondence.

Jorge Pedrón Torrecilla
Universitat Politècnica de València. Ed. 8G. Bio-ITACA
Camino de Vera s/n. CP: 46022. Valencia, Valencia, Spain
jorpedto@itaca.upv.com